

Numerical study on influences of bed resettling, breeding zone orientation, and purge gas on temperatures in solid breeders

Jon T. Van Lew*, Alice Ying, Mohamed Abdou

UCLA, MAE Department, 44-114 Engineering IV, 420 Westwood Plaza, Los Angeles, CA 90095-1597, USA



HIGHLIGHTS

- Volume-conserving pebble fragmentation model in DEM to study thermomechanical responses to crushed pebbles in ensembles.
- Parametric studies of ITER-relevant pebble beds with coupled CFD-DEM models.
- Finding breeder temperatures are complex functions of orientation, fragmentation size, and packing fraction.
- Recommendations of breeder unit orientation are given in terms of material selection.

ARTICLE INFO

Article history:

Received 29 August 2015

Received in revised form 3 February 2016

Accepted 17 February 2016

Available online 8 March 2016

Keywords:

Coupled CFD-DEM
Granular heat transfer
Granular crushing
Ceramic breeder

ABSTRACT

We apply coupled computational fluid dynamics and discrete element method (CFD-DEM) modeling tools with new numerical implementations of pebble fragmentation to study the combined effects of granular crushing and ensemble restructuring, granular fragment size, and initial packing for different breeder volume configurations. In typical solid breeder modules, heat removal from beds relies on maintaining pebble-pebble and pebble-wall contact integrity. However, contact is disrupted when an ensemble responds to individually crushed pebbles. Furthermore, restructuring of metastable packings after crushing events are, in part, dependent on gravity forces acting upon the pebbles. We investigate two representative pebble bed configurations under constant volumetric heat sources; modeling heat removed from beds via inter-particle conduction, purge gas convection, and contact between pebble beds and containers. In one configuration, heat is removed from at walls oriented parallel to the gravity vector (no gap formation possible); in the second, heat is removed at walls perpendicular to gravity, allowing for the possibility of gap formation between bed and wall. Judging beds on increase in maximum temperatures as a function of crushed pebble amount, we find that both pebble bed configurations to have advantageous features that manifest at different stages of pebble crushing. However, all configurations benefit from achieving high initial packing fractions.

© 2016 Elsevier B.V. All rights reserved.

1. Introduction

Pebble beds of lithium ceramics exist in candidate designs of nuclear fusion demonstration reactors and tritium breeding modules in ITER. For optimum tritium release, ceramic pebble beds have relatively narrow operational temperature windows that must be maintained. Bed temperatures are regulated via coolant running through the structural material, heat is transported from bed to structure, in part, from pebble-wall contact conduction. Therefore maintaining physical contact between granular material

and structural material is necessary for heat outflow from the bed. Temperature prediction and control is of utmost importance for reliable tritium release and energy production in a fusion reactor's ceramic pebble bed, but current models lack predictive capability with full consideration for granular crushing, resettling, and interstitial gas.

The discrete element method (DEM) has emerged as an extremely powerful approach for interrogating and modeling evolving, transient, pebble-scale information in packed beds. DEM models have also been successfully coupled to volume-averaged computational fluid dynamics (CFD) models; coupled CFD-DEM models are capable of predicting temperature distributions in ceramic pebble beds with the slow-flowing interstitial purge gas while continuing to provide useful information on pebble-scale

* Corresponding author.

E-mail address: jtvanlew@fusion.ucla.edu (J.T. Van Lew).

interactions. In this paper, we employ coupled CFD-DEM models with fragmentation modeling schemes to study the combined effects of initial packing fraction, crushed pebbles, gravity-influenced bed resetting after crushing events, and orientation of containing structures on temperature distributions in packed beds.

2. Numerical methodology

With our DEM model, each pebble is treated as a perfectly elastic, smooth, non-cohesive sphere with mechanical interactions described by Hertzian contact laws where a conductance of heat is permitted through the contact area (see Ref. [1] and the references therein). Pebble interaction with fluid flow is captured via: a fluid drag coefficient, as calculated from the local fluid velocity, applied over pebble surfaces; and a local Nusselt number, calculated from passing fluid temperatures and velocities. The numerical technique is described in more detail in a previous study [2]. The position and temperature of every particle evolve with the explicit velocity-Verlet time marching scheme.

The fluid-phase flow and temperature fields are calculated from transient, volume-averaged formulations of Navier-Stokes and energy equations calculated in computational cells that are overlaid on the DEM domain. Two-way coupling with the DEM model is achieved with a drag force source term in Navier-Stokes and an energy source term in the energy equation of the gas phase which are volume-averaged summations of the drag and heat transfer coefficients calculated with DEM for all pebbles. We employ modeling tools of our previous study in which more details can be found [2].

2.1. Simulation domain, boundary conditions, and material properties

Two ITER-relevant volumes are considered in this study, sketched in Fig. 1a and b. They are differentiated from each other by gravity's direction in the configuration. Because of their similarity, we use generic coordinate systems (χ , ζ). Thus χ -configurations, shown in Fig. 1a, have $\chi=y$ and $\zeta=x$ while ζ -configurations, Fig. 1b, have $\chi=x$ and $\zeta=y$. The ζ -configuration in this study is meant to represent the orientation of European Union's TBM [3], while the χ configuration is an orientation adopted by many other current TBM designs in ITER [4,5].

In terms of the generic coordinates, outflow of bed heat to coolant is along ζ . Constant temperature boundaries, T_w , exist at the edges of that dimension. As sketched in Fig. 1, gravity resetting

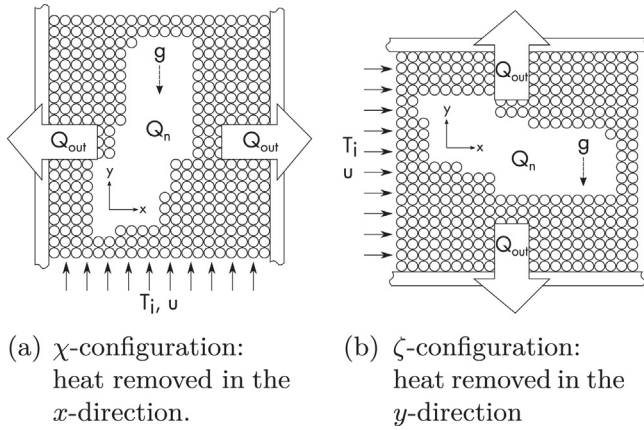


Fig. 1. Sketches of the two breeder orientations show that gravity settling will not allow gaps between pebbles and walls in the χ -configuration. However for the ζ -configuration, gravity-induced resetting can create a gap between pebbles and upper wall.

Table 1

Mechanical and thermal properties of ceramic pebbles in the DEM domain. Aside from E_s , properties come from [7] with $\epsilon=0.2$.

Property	Symbol	Value
Young's modulus (GPa)	E_s	60
Poisson ratio	ν_s	0.24
Thermal conductivity ($\text{W m}^{-1} \text{K}^{-1}$)	k_s	1.79
Diameter (m)	d_p	0.001
Pebble-pebble friction coefficient	μ_s	0.2
Pebble-wall friction coefficient	μ_w	0.2
Heat capacity ($\text{J kg}^{-1} \text{K}^{-1}$)	c_s	1.45×10^3
Thermal expansion coefficient (K^{-1})	β_s	1.77×10^{-5}
Density (kg m^{-3})	ρ_s	3.44×10^3

in the χ configuration will not allow gap formation between bed and wall. However, in the ζ -config it is possible for a gap to form between top coolant walls and pebbles after gravity resettling. A constant nuclear heat rate was applied to every particle in the bed which is representative of the highest source term anticipated in current ITER designs of solid breeder blankets, $q'''=8 \times 10^6 \text{ W m}^{-3}$.

The simulation consists of pebbles of diameter $d_p = 1 \text{ mm}$, in beds filled to two initial packing fractions, $\phi_{1,2} = 62, 64\%$. Mechanical properties of the pebbles are given in Table 1. To note is the Young's modulus chosen for pebbles in this study. In a past experimental study, Van Lew et al. found that individual pebbles behaved in a manner indicative of having a Young's modulus from 20 to 60% of values reported in literature for sintered blocks of Li_2TiO_3 and Li_4SiO_4 [6]. Therefore to maintain some generality to this study, we have chosen a Young's modulus at a nominal value of $E = 60 \text{ GPa}$ to generically represent either ceramic pebble.

Pebble bed widths in ζ are 20 mm, a size comparable to breeding volumes of many ITER TBM designs [3–5]. Bed depths (in the z -direction, in/out of the page in Fig. 1a and b) are 5 mm, with periodic boundary conditions. Bed lengths in χ vary to accommodate 6000 pebbles, initially, with given initial packing fractions; the length is approximately 50 mm. Virtual walls are placed at extents of χ and ζ dimensions. Walls in ζ had constant temperature boundaries of $T_{w,s}$, all walls have mechanical and thermal properties of structural steel, given in Table 2.

Fluid domains, overlaid on DEM pebbles, have fluid inlet and outlet regions of lengths 10 mm and approximately 51 mm, respectively. The side walls of the fluid domain were adiabatic in inlet and outlet regions and had constant temperature boundaries where they contacted the pebble bed, $T_{w,f}$. Fluid entered with a constant velocity magnitude of 5 cm s^{-1} and constant temperature T_i . At present, temperature-dependencies of helium properties have not been incorporated into the model. Over the range of 400–900 °C, increases in helium momentum and thermal diffusivities are both essentially linear and thus an arithmetic mean for properties over that range is used as a first approximation. Future models will incorporate temperature-dependence of fluid properties. Fluid transport properties are given in Table 3.

2.2. Modeling crush events

Models have been proposed in the past which translate experimental measurements of granular crushing into contact forces in an ensemble to predict granular crushing, e.g. Refs. [6,8–11], but

Table 2

Mechanical and thermal properties and boundary conditions of structural container in the DEM domain.

Property	Symbol	Value
Young's modulus (GPa)	E_w	175.
Poisson ratio	ν_w	0.30
Thermal conductivity ($\text{W m}^{-1} \text{K}^{-1}$)	k_w	29.0
Wall temperature (K)	$T_{w,s}$	573

Table 3

Transport properties of helium and boundary conditions in the CFD domain; mean values over the temperature range 400–900 °C.

Property	Symbol	Value
Thermal conductivity ($\text{W m}^{-1} \text{K}^{-1}$)	k_f	3.40×10^{-1}
Heat capacity ($\text{J kg}^{-1} \text{K}^{-1}$)	c_f	5.19×10^3
Density (kg m^{-3})	ρ_f	5.38×10^{-2}
Kinematic viscosity (m s^{-2})	λ_f	8.52×10^{-4}
Thermal diffusivity (m s^{-2})	α_f	1.28×10^{-3}
Wall temperature (K)	$T_{w,f}$	573
Inlet temperature (K)	T_i	573

no validation has set any model apart as yet. Here, packed beds experience artificial pebble-crushing events for which a chosen percentage, η , of initial pebbles (at randomized locations) fragment. Four pebble crush percentages are used: $\eta = 0, 1, 3, 5\%$. Numerical models of crush events themselves have received attention. Annabattula et al. attempted to model a crushing event as either a reduction in radius of the crushed pebble or a reduction in Young's modulus [12–14]. Van Lew et al. made similar simplifications when they considered a crushed pebble as being removed from the force network, thus being removed from the DEM domain [1].

In this work, we replace a parent pebble of radius r with N_c smaller daughter fragments, each of equal radius, r_c . After a crushing event, fragments are free to resettle through interstitial gaps in the pebble bed and original pebbles respond in kind with rearrangement into a new metastable packing structure. To conserve volume between pre- and post-crush, we can relate the number of daughter fragments to the radius ratio between fragments and parent, $r^* = r_c/r$, as $N_c = (1/r^*)^3$. Conservation of energy of crush event is enforced by setting the temperature of daughter fragments to the parent pebble at the moment of crushing.

Experimental studies of crushing brittle pebbles show many different modes of fragmentation, often with highly irregular sizes (see e.g. Ref. [15]). As a first effort, we compare the effect of fragmentation size by studying two different values, $r_1^* = 0.352$ and $r_2^* = 0.2$ which results in $N_{c,1} = 23$ and $N_{c,2} = 125$ daughters per crushed parent (at $\eta = 5\%$, for r_2^* the system expands to 43,200 pebbles).

As a consequence of volume conservation in a fragmentation event, the daughter fragments naturally cannot fit into the parent pebble without overlap. Numerically, in our fragmentation procedure, overlap and the associated high contact forces between the daughter fragments is permitted. Directly following a fragmentation event, a cut-off distance is applied to the velocity-Verlet integration of daughter fragments which prevents instabilities in position; e.g. in any given timestep fragments are only allowed to travel x_{cutoff} , regardless of the distance calculated in integration. A short time is permitted for the daughter fragments to relax away from the highly overlapped state; relaxation time was a function of number of pebble fragments and pebble fragment size. Contact forces in the system were monitored and when average values returned to pre-fragmentation levels, the relaxation procedure concluded, cut-off distance was removed, and standard velocity-Verlet integration of daughter pebbles was reinstated.

3. Numerical solvers

Pebble contact and heat transfer models are packaged into LIGGGHTS, a modification of LAMMPS with powerful additions for granular material [16,17]. The helium fluid domain is modeled with a modified PISO solver in the framework of OpenFOAM® from OpenCFD, Ltd. [18]. Coupling between LIGGGHTS and OpenFOAM is accomplished with open-source, modular C++ libraries maintained by CFDEM Project [19].

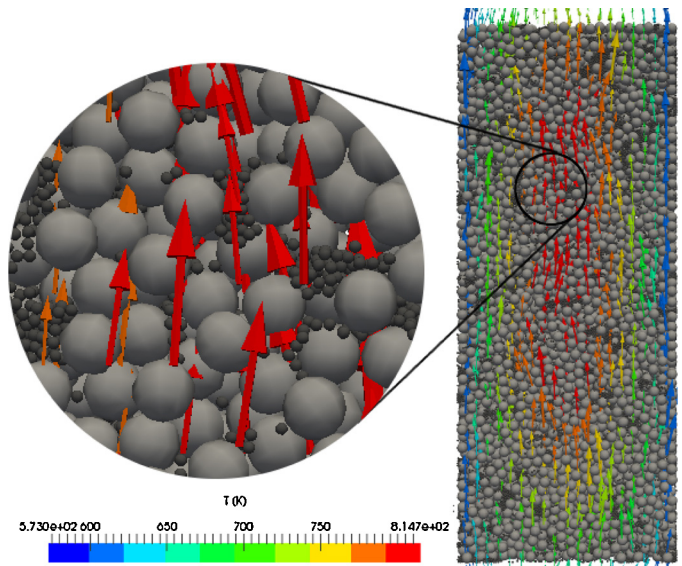


Fig. 2. Showing the case for $\phi_2 = 0.64$, $\eta = 5\%$ with fluid velocity vectors colored by temperature. Inset image reveals size discrepancies between fragments and pebbles and the ensemble interaction with fluid flow.

4. Results and discussion

In Fig. 2, a bed of 64% initial packing with 5% of pebbles broken into fragments of size $r_2^* = 0.2$ is shown; vectors of flow field, colored by fluid temperature, are seen moving through the bed. The inset image qualitatively demonstrates how the fluid field aids in equilibrating temperatures of fragments with neighboring larger pebbles.

Several cross-sections are created at mid-planes in z . Representative results are taken from 64% packings of ζ - and χ -configurations and compared against their respective $\eta = 5\%$, r_2^* conditions, shown in Figs. 3 and 4. The numbered zones of the beds will be discussed shortly.

Wall offset-temperatures ($T - T_w$) in beds are found in slices of width $\Delta\zeta$ along ζ . Pebble-weighted mean values are found as $\langle T \rangle =$

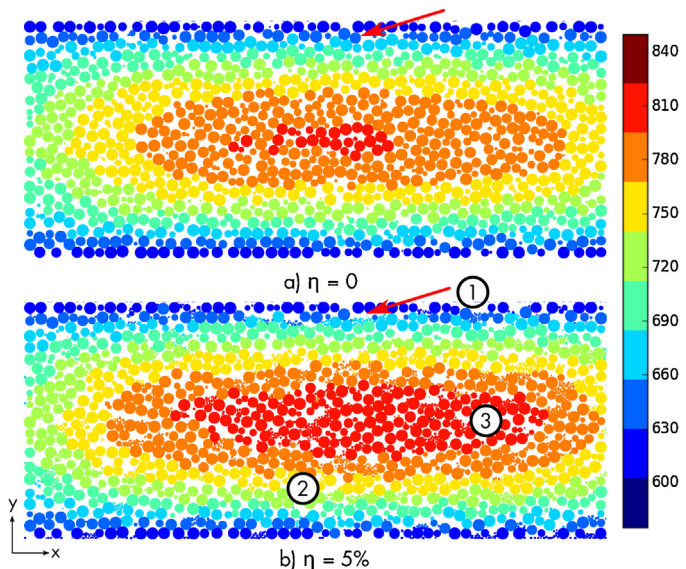


Fig. 3. Cuts at the mid-plane of z for ζ -config beds. (a) Bed initially packed to ϕ_2 , and (b) bed with crushing of η_5 pebbles with particle size r_2^* . Three important zones have been identified.

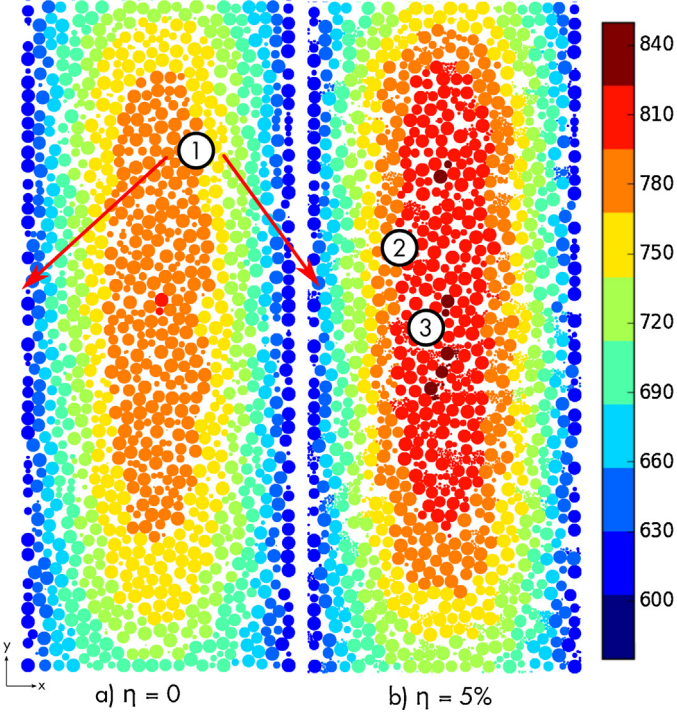


Fig. 4. Cuts at the mid-plane of z for χ -config beds. (a) Bed initially packed to ϕ_2 , and (b) bed with crushing of η_5 pebbles with particle size r_2^* . Three important zones have been identified.

$\frac{1}{V_n} \sum_j^n (T_j - T_w)V_j$, for n pebbles of temperature T_j consuming a total volume V_n in the slice. Demonstrative cases of $\phi_2 = 0.64$ with $r_2^* = 0.2$ are given in Fig. 5 as functions of granular crushing percentage.

Following the formulations described by Gan and Kamlah [20], and Gan et al. [21], we report the overall hydrostatic pressure of pebble beds, $p = \sigma_{ii}/3$, at steady-state heating. The values are normalized against initial ($\eta = 0$) beds for respective configurations. Hydrostatic pressure is given in Fig. 6. A total mean bed temperature is found from all pebbles in the system as $\langle T \rangle_{tot} = \frac{1}{V_N} \sum_j^N (T_j - T_w)V_j$ where N is the total number of ensemble pebbles. The total mean bed temperature is also normalized against initial packing cases of each respective set of beds. Results for all beds are given in Fig. 7. Maximum temperature rises of every bed are also found, $T_m = \max(T) - T_w$, and normalized against the maximum temperature in the initial packing of each respective set of beds. To avoid

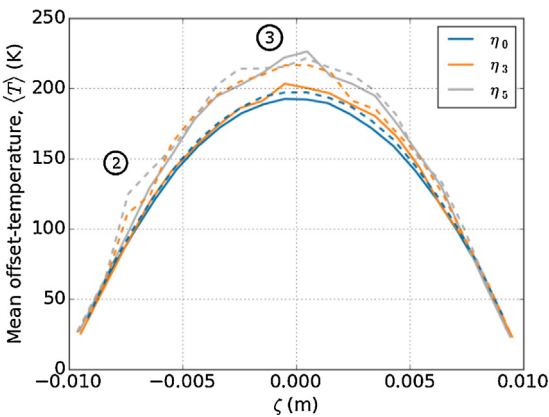


Fig. 5. Mean offset-temperature profiles, $\langle T \rangle$, along ξ in beds with initial packing fractions $\phi_2 = 0.64$, fragmentation sizes were r_2 . Solid lines are χ configurations, dashed lines are ζ configurations. Fragmentation settling of ζ -configs are seen in 'lumps' near Zone (2) and in the χ -config spike in Zone (3).

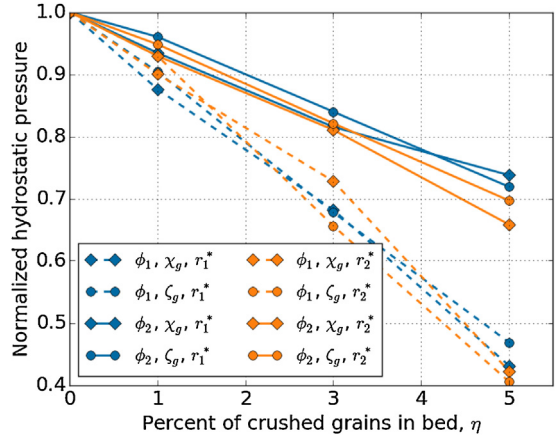


Fig. 6. Dashed lines represent the lower packing fraction, $\phi_1 = 0.62$, solid lines are $\phi_2 = 0.64$. Markers are: \diamond for ζ -config, \blacklozenge for χ -config. Color differentiates the fragment radius ratio. Contact force relaxation is more rapid for lower packing fractions. (For interpretation of the references to color in this figure legend, the reader is referred to the web version of this article.)

aberrant results from a bed which might have a single, very high temperature pebble, the maximum temperature, $\max(T)$, is calculated as a mean value of the 50 highest temperature pebbles. The results are given in Fig. 8. In addition to total mean bed temperature, maximum temperature rise is also an important factor in evaluation of a pebble bed.

Lastly, we consider how far pebble fragments travel in the bed after a crushing event. Total displacements from the moment of crush event to final resting, $|\Delta h|$, are normalized against the original pebble diameter, $|\Delta h|/d_p$. Histograms for 64% packing fractions of χ - and ζ -configurations at 5% pebble crushing with fragment sizes r_2^* are given in Fig. 9. These two beds saw the most settling, all other beds tested saw considerably less fragment travel.

Analyzing results of all the pebble beds in this study revealed two main contributors to bed temperatures with resettling from pebble crushing: final settling location of fragment particles and overall contact force relaxation. The two interacting contributors were found to be expressed to different extents depending on crush amount and bed configuration.

Hydrostatic pressure (a global measure of inter-particle contact forces) is predominately a function of initial packing fraction alone,

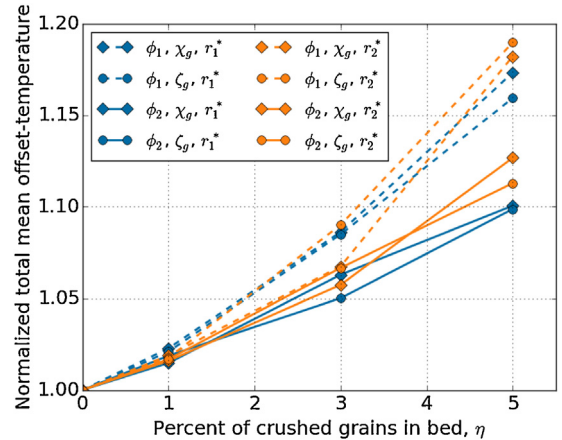


Fig. 7. Dashed lines represent the lower packing fraction, $\phi_1 = 0.62$, solid lines are $\phi_2 = 0.64$. Markers are: \diamond for ζ -config, \blacklozenge for χ -config. Color differentiates the fragment radius ratio. Lower packing fraction is the most dominant parameter for overall bed temperature. Amongst the same packing fraction, fragment size is most influential factor. (For interpretation of the references to color in this figure legend, the reader is referred to the web version of this article.)

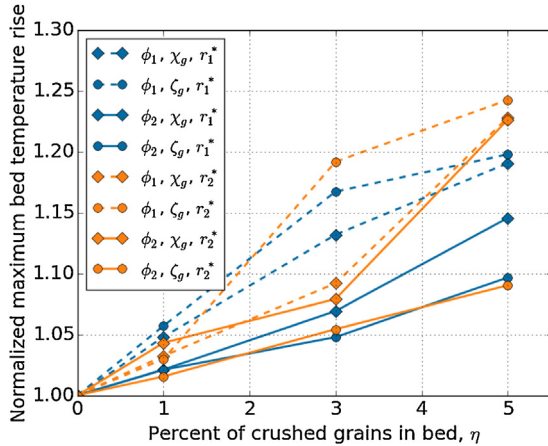


Fig. 8. Dashed lines represent the lower packing fraction, $\phi_1 = 0.62$, solid lines are $\phi_2 = 0.64$. Markers are: \circ for ζ -config, \diamond for χ -config. Color differentiates the fragment radius ratio. The dominant parameter influencing maximum bed temperature varies as a function of the number of crushed pebbles in the bed. (For interpretation of the references to color in this figure legend, the reader is referred to the web version of this article.)

as seen in Fig. 6. Smaller initial packing fractions had their internal hydrostatic pressure reduced more rapidly as pebbles crushed in the ensemble. Breeder orientation appears to have less impact on stress relief than size of crush fragments. Due to the interconnected nature of the force network, and geometry of beds studied here, resettling in beds and contact force relaxation is uniform throughout the beds. Thus we expect reductions in contact forces to directly result in an overall increase of bed temperatures. This is reflected in the curves of Fig. 7. Total mean temperatures of $\phi_1 = 0.62$ beds increased between 16 and 19% at $\eta = 5\%$. Yet beds initially packed to $\phi_2 = 0.64$ increased by only 10–13% at the same value of crushed pebble amount.

Fragment settling location, on the contrary, is strongly dependent on fragment size and breeder orientation. Larger pebble fragments generally did not travel far, settling loosely in regions near the point of fragmentation. Smaller fragments were seen to be capable of traveling much further through interstitial gaps between pebbles before also coming to rest with loose settling. The looseness of the fragment settling is indicated by their ensemble-average coordination number (counting only the fragments) for r_1^* and r_2^* , respectively, as $\langle Z \rangle = 3.2$ and $\langle Z \rangle = 2.8$. Contacts with walls or floors are not counted in this coordination number. A consequence of loose packings of fragments is poor thermal conductance to neighboring pebbles. Fragment temperatures are therefore mostly regulated

by convection with interstitial helium and their influence on bed temperatures is much more complex.

To identify the effects of fragment settling, we look to Fig. 9 and the several zones demarcated in the results of Figs. 3 and 4. The majority of fragments, even in this case of smallest fragment size and largest crushing amount, remain approximately at the location of the parent pebble; for both configurations, approximately 60% travel less than 1 pebble diameter (1 mm). However, in both configurations, approximately 8% of fragments travel more than 2 diameters, and those pebbles have a significant impact on the ensembles overall thermal response.

In ζ -configuration beds, pebbles traveling more than a few pebble diameters will move between colored isotherms drawn in Fig. 3. For example we can see the fragment group identified in Zone (1) as moving downward, away from the top wall. Similarly, when pebbles in Zone (3) are crushed, some of the fragments tumble downward into Zone (2) before coming to rest where they continue to receive volumetric heating. Thus the fragments, with poor thermal conductance, increase heating in the regions where they settle. The effect is seen in the $\eta = 3$, 5% temperature profiles in Fig. 5 that are asymmetric with lower temperatures in the top half (above Zone (3)) and higher temperatures in the region near Zone (2).

In contrast, χ -config beds respond much differently to pebble fragment settling. We again see from cross-sections in Fig. 4 a pebble identified in Zone (1) that breaks but remains in that zone after settling. The trend continues in other regions of the bed. When pebbles are crushed in the χ -config beds, gravity causes them to fall downward but remain generally in the same isotherm, as drawn in Fig. 4. According to Fig. 5, the effect of pebble crushing has little effect up to 3% of damaged pebbles. But suddenly at $\eta = 5\%$, the combination of reduced overall bed pressure and fragmentation heating causes the maximum bed temperature to jump above all other $\phi = 64\%$ beds (see Figs. 5 and 8). The temperature increase in this χ -config bed is due to the accumulation of pebble fragments that remain in Zone (3), only tumbling to lower heights. Helium that enters the χ -configuration bed reaches higher temperatures more quickly due to the increased heating from fragments which settled at lower heights of y . Helium then continues to heat from the many fragments in Zone (3) which ultimately results in the highest maximum bed temperatures (for the given packing fraction). This can also be seen with comparison between Figs. 3 and 4: the χ -config bed reaches the 780 K contour at a much lower height than the ζ -configuration.

5. Conclusions

We conducted several multi-scale simulations of granular heat transfer using coupled CFD-DEM simulations of representative tritium-breeding ceramic pebble bed volumes with parametric variations of: bed orientation with respect to gravity, pebble crushing amount, initial packing fraction, and crushed fragmentation size.

There was one general trend observed that reiterates past conclusions from solid breeder research. Namely, more persistent behavior is witnessed in pebble beds with higher initial packing fractions. In this study, the most dominant parameter observed to affect temperatures in pebble beds was the initial packing fraction: beds with higher initial packing fraction had smaller increases in bed temperatures due to pebble crushing. We therefore conclude that manual densification, from either long-term vibration packing or load-induced pre-compaction, must be done to ceramic pebble bed volumes to gain some temperature control during operation in a fusion reactor. To achieve packing fractions of 64% in the relatively small sizes of this study, for example, a load of over 1 MPa was

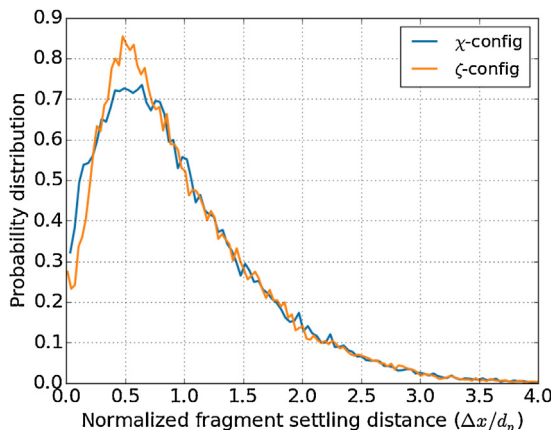


Fig. 9. Normalized displacement histograms for fragment sizes of $r_2^* = 0.2$ with $\eta = 5\%$. χ -config: 59.7% of fragments travel up to 1 mm and 8.2% travel more than 2 mm; ζ -config: 60.7% of fragments travel up to 1 mm, 7.9% travel more than 2 mm.

necessary. In the assembly of tritium breeding modules, it must be kept in mind that similar pre-compaction may need to be performed.

As stated earlier, a concern with the ζ design is the possibility of gap formation between pebble bed and upper walls after bed resettling, particularly after pebble fragmentation. In this study, we found pebble beds initially packed to $\phi=62\%$ experienced the highest increases in both total average bed temperature as well as maximum temperature rise. The comparably looser packing allowed a quick reduction in hydrostatic pressures and consequently a reduction in heat conduction to the upper wall. Nevertheless, no gaps were detected even at 5% of pebbles crushed. However, temperatures in pebble beds packed to 64% showed a resistance to fragmentation; overall average temperatures were comparable to χ -configurations, and in fact these EU-style beds had the lowest maximum temperatures for beds with many crushed pebbles. We showed that freedom of fragments to travel between zones in these beds prevented a build-up of loose fragments (and thereby avoided build-up of heating) in the hottest regions.

As for the χ -configurations, we found that when there were not many broken pebbles ($\eta \leq 3\%$), these beds generally had lower temperatures in comparison to similar ζ -config beds. But as η went above 3% for many of the beds, the averaged bed temperature and, importantly, the maximum temperature rise actually jumped above the ζ -configurations. We showed that for these beds it was the inability for fragments to move between zones which left many small fragments to settle in the hottest region, further contributing to heating.

From the results we have shown, it is obvious that pebble crushing and bed resettling effects on temperature are complicated, non-linear responses and are particular to breeder design and ceramic material employed. We found indications of certain operational spaces for which different designs responded less severely to pebble crushing. For instance, from the sole point of view of temperature response in pebble beds, if one were to employ a material known to have a limited crush strength, one might accept that many pebbles could break (at least up to 5%, as studied here) over the life of the breeder and choose to employ the ζ -style which avoided large increases in temperature after long operation of the breeder. Alternatively, if one had a ceramic material with a larger crush strength, the χ -design would be preferable as it generally retained lower overall and maximum bed temperatures when fewer pebbles in the ensemble were crushed.

It must be pointed out that the findings discussed here are concerned primarily with temperature distribution, without consideration for other consequences of pebble crushing such as blocking of helium purge, and thereby tritium extraction, by clogging from fragment dust or particulates. Clogging of purge flow is specific to each pebble bed design and must receive future attention in its own right.

This study was performed on some generic geometries and has provided some generalized conclusions. But in light of the pebble beds' complex responses, as breeder designs continue to evolve into their final form before deployment in ITER, CFD-DEM models

should continuously be employed to study the specific thermomechanical responses to pebble crushing and bed resettling unique to each design.

Acknowledgements

This work was performed with support from the US Department of Energy, Office of Fusion Energy Sciences, under Grant No. DE-FG02-86ER52123.

References

- [1] J.T. Van Lew, A. Ying, M.A. Abdou, A discrete element method study on the evolution of thermomechanics of a pebble bed experiencing pebble failure, *Fusion Eng. Des.* 89 (2014) 1151–1157.
- [2] J.T. Van Lew, A. Ying, M. Abdou, Coupling discrete element models of ceramic breeder pebble beds to thermofluid models of helium purge gas using volume-averaged Navier–Stokes and the Lattice–Boltzmann Method, *Fusion Sci. Technol.* 68 (2015).
- [3] F. Hernández, M. Kolb, M. Ilić, a. Kunze, J. Németh, a. Von Der Weth, Set-up of a pre-test mock-up experiment in preparation for the HCPB Breeder Unit mock-up experimental campaign, *Fusion Eng. Des.* 88 (2013) 2378–2383.
- [4] S. Cho, M.-Y. Ahn, D.H. Kim, E.S. Lee, S. Yun, N.Z. Cho, K.J. Jung, Current status of design and analysis of Korean Helium-Cooled Solid Breeder Test Blanket Module, *Fusion Eng. Des.* 83 (2008) 1163–1168.
- [5] K.M. Feng, C.H. Pan, G.S. Zhang, T.Y. Luo, Z. Zhao, Y.J. Chen, Y.J. Feng, X.F. Ye, G. Hu, K.H. He, R.W. Niu, Z.X. Li, P.H. Wang, B. Xiang, L. Zhang, Q.J. Wang, F.C. Zhao, Q.X. Cao, F. Wang, T. Yuan, G.Y. Zheng, Y. Liu, Y. Zhong, M.C. Zhang, Progress on design and R&D for helium-cooled ceramic breeder TBM in China, *Fusion Eng. Des.* 87 (2012) 1138–1145.
- [6] J.T. Van Lew, Y.-H. Park, A. Ying, M. Abdou, Modifying Young's modulus in DEM simulations based on distributions of experimental measurements, *Fusion Eng. Des.* (2015).
- [7] P.J. Gierszewski, Review of properties of lithium metatitanate, *Fusion Eng. Des.* 39–40 (1998) 739–743.
- [8] Y. Gan, M. Kamlah, H. Riesch-Oppermann, R. Rolli, P. Liu, Crush probability analysis of ceramic breeder pebble beds under mechanical stresses, *J. Nucl. Mater.* (2010) 10–13.
- [9] A.R. Russell, D. Muir Wood, M. Kikumoto, Crushing of particles in idealised granular assemblies, *J. Mech. Phys. Solids* 57 (2009) 1293–1313.
- [10] S. Zhao, Y. Gan, M. Kamlah, Spherical ceramic pebbles subjected to multiple non-concentrated surface loads, *Int. J. Solids Struct.* 49 (2012) 658–671.
- [11] R.K. Annabattula, Size-dependent crush analysis of lithium orthosilicate pebbles, *Fusion Sci. Technol.* 66 (2014).
- [12] R.K. Annabattula, Y. Gan, M. Kamlah, Mechanics of binary and polydisperse spherical pebble assembly, *Fusion Eng. Des.* (2012) 2–7.
- [13] S. Zhao, Y. Gan, M. Kamlah, Failure initiation and propagation of Li_4SiO_4 pebbles in fusion blankets, *Fusion Eng. Des.* 88 (2013) 8–16.
- [14] R.K. Annabattula, Y. Gan, S. Zhao, M. Kamlah, Mechanics of a crushable pebble assembly using discrete element method, *J. Nucl. Mater.* 430 (2012) 90–95.
- [15] S. Wu, K. Chau, T. Yu, Crushing and fragmentation of brittle spheres under double impact test, *Powder Technol.* 143–144 (2004) 41–55.
- [16] S. Plimpton, Fast parallel algorithms for short-range molecular dynamics, *J. Comput. Phys.* 117 (1995) 1–19.
- [17] C. Kloss, C. Goniva, A. Hager, S. Amberger, S. Pirker, Models, algorithms and validation for opensource DEM and CFD-DEM, *Prog. Comput. Fluid Dyn.* 12 (2012) 140–152.
- [18] OpenCFD Ltd., OpenFOAM – The Open Source CFD Toolbox, 2014.
- [19] C. Goniva, C. Kloss, N.G. Deen, J.A. Kuipers, S. Pirker, Influence of rolling friction on single spout fluidized bed simulation, *Particuology* 10 (2012) 582–591.
- [20] Y. Gan, M. Kamlah, Discrete element modelling of pebble beds: with application to uniaxial compression tests of ceramic breeder pebble beds, *J. Mech. Phys. Solids* 58 (2010) 129–144.
- [21] Y. Gan, F. Hernandez, D. Hanaor, R.K. Annabattula, M. Kamlah, P. Pereslavtsev, Thermal discrete element analysis of EU solid breeder blanket subjected to neutron irradiation, *Fusion Sci. Technol.* 66 (2014).